# Control Strategies Based on Symmetrical Components for Grid-Connected Converters Under Voltage Dips

Salvador Alepuz, *Member, IEEE*, Sergio Busquets-Monge, *Member, IEEE*, Josep Bordonau, *Member, IEEE*, Juan A. Martínez-Velasco, *Member, IEEE*, César A. Silva, *Member, IEEE*, Jorge Pontt, *Senior Member, IEEE*, and José Rodríguez, *Senior Member, IEEE*

***Abstract*—Low-voltage ride-through (LVRT) requirements demand wind-power plants to remain connected to the network in presence of grid-voltage dips. Most dips present positive-, negative-, and zero-sequence components. Hence, regulators based on symmetrical components are well suited to control grid-connected converters. A neutral-point-clamped topology has been considered as an active front end of a distributed power-generation system, following the trend of increasing power and voltage levels in wind-power systems. Three different current controllers based on symmetrical components and linear quadratic regulator have been considered. The performance of each controller is evaluated on LVRT requirement fulfillment, grid-current balancing, maximum grid-current value control, and oscillating power flow. Simulation and experimental results show that all three controllers meet LVRT requirements, although different system performance is found for each control approach. Therefore, controller selection depends on the system constraints and the type of preferred performance features.**

***Index Terms*—Distributed power generation, grid interface, multilevel conversion, three-level inverter, wind-power system.**

## I. Introduction

In recent years, wind-energy power-generation systems have increased significantly their capacity. This growth is particularly important in Europe, where the installed wind-power capacity at the end of 2007 was 57 GW [1]. This amount exceeds by far the joint objective of 40 GW in 2010 given by the European Commission in 1997 [2]. In the world, more than 19 GW (25.9% growth) were installed in 2007 [1], increasing the worldwide wind-power capacity up to 93.6 GW.

In this scenario, the influence of wind plants in the power system operation becomes more important. For that reason, power systems operators have updated gradually their grid connection requirements (GCRs) for generators [3]–[6]. The former GCR allows the disconnecting of wind-power plants in the presence of grid disturbances. Nowadays, with a significant percentage of electricity generated by wind plants, power systems operators prefer to include wind-power plants in the transient operation control of the overall power system. Low-voltage ride-through (LVRT) requirements demand wind-power plants to remain connected in the presence of dips, contributing to keep the grid voltage and frequency stable.

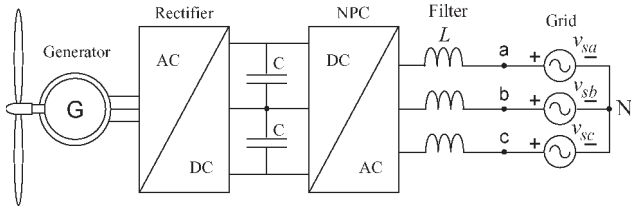


Fig. 1. Wind generator connected to the grid through a full-power converter.

Most voltage dips caused by network faults present positive-, negative-, and zero-sequence components [7]. Hence, it is reasonable to use these symmetrical components in the control of grid-connected voltage source converters (VSCs) [8], [9] under unbalanced network condition. Some control approaches for grid-connected converters applied to distributed power generation can be found in the literature [10]. Balanced grid currents under distorted network voltages are attained in [11], with a positive-sequence current controller and negative-sequence grid-voltage feedforward, considering a VSC connected to the grid through an inductor–capacitor–inductor (LCL) filter. In [12], two different dual current controllers achieve either dc-link voltage-ripple cancellation or to nullify active power ripple delivered to the grid. A comparison of the preceding current controllers under different dips is found in [13] for a VSC and an inductor (L) filter and for a neutral-point-clamped (NPC) topology with an LCL filter in [14]. The fulfillment of the LVRT requirement is not studied in the aforementioned works.

As result of the increasing power in wind turbines, current trends in wind-power technology point to step up the voltage level, in order to reduce current ratings and cabling costs. Therefore, back-to-back multilevel converters [15]–[19] are suitable to connect variable-speed wind turbines to the grid. Hence, this paper considers only wind-power plants implemented with a full-power NPC converter [20] (see Fig. 1).

Manuscript received May 28, 2008; revised February 25, 2009. First published March 16, 2009; current version published June 3, 2009. This work was supported in part by the Ministerio de Educación y Ciencia, Spain, under Grant TEC2005-08042-C02-02/MIC, in part by the Programa Bicentenario de Ciencia y Tecnología (CONICYT), Chile, in part by Millennium Nucleus Industrial Electronics and Mechatronics (MIDEPLAN), Chile, in part by Fundación Andes, Chile, and in part by the Universidad Técnica Federico Santa María, Chile.

S. Alepuz, S. Busquets-Monge, and J. Bordonau are with the Department of Electronic Engineering, Technical University of Catalonia, 08028 Barcelona, Spain (e-mail: alepuz@eupmt.es).

J. A. Martínez-Velasco is with the Department of Electrical Engineering, Technical University of Catalonia, 08028 Barcelona, Spain (e-mail: martinez@ee.upc.edu).

C. A. Silva, J. Pontt, and J. Rodríguez are with the Departamento de Electrónica, Universidad Técnica Federico Santa María, Valparaíso, Chile (e-mail: jpo@elo.utfsm.cl).

Digital Object Identifier 10.1109/TIE.2009.2017102

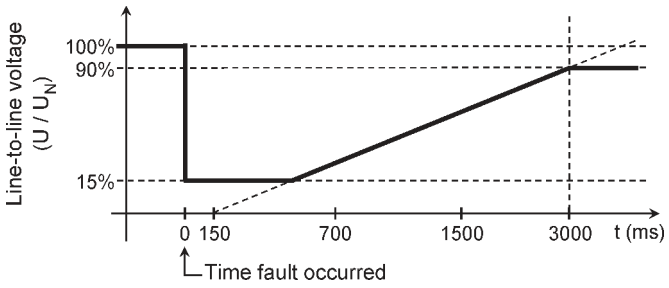


Fig. 2. Voltage-limit curve to allow wind-turbine disconnection.

This paper is focused on LVRT requirements fulfillment for the system shown in Fig. 1. The dc-link is assumed constant, both in steady state [18], [21], [22] and under grid fault [21]–[24]. Therefore, grid- and generator-side operations are decoupled, and only the grid-side converter control is considered, i.e., the dc-link brake chopper [21], [23], [24], the generator-side converter, and their respective controllers [16], [17], [21]–[24] are not included in the model.

In this paper, three different current-controller strategies [11], [12] for the grid-side converter shown in Fig. 1 are evaluated considering that, when a grid fault appears, the objectives of a grid-connected VSC controller are as follows: to deliver average active and reactive power to the grid as specified in the GCR, to minimize instant active and reactive power ripple, to deliver balanced grid currents, to control maximum grid-current value, and to minimize dc-link voltage ripple. Therefore, system performance has been evaluated considering not only LVRT requirement specifications but also all the other controller objectives aforementioned.

Current controllers have been implemented using linear quadratic regulator (LQR) [25], in order to take advantage of the multivariable nature of the system. However, this is not a key point, and other current-control techniques can be also applied; for instance, current controllers implemented using two proportional–integral current controllers in the $d$–$q$ frame with cross-coupled terms.

This paper is organized as follows. Section II details the LVRT requirements. A description of the system, its model, and equations are given in Section III. The three controllers under study, together with the LQR controller calculation, are described in Section IV. Validation by comparing simulation and experimental results is found in Section V. Additional simulation results for a high-power system are shown in Section VI. Finally, conclusions are presented in Section VII.

## II. LVRT Requirements

When a grid-voltage dip appears, LVRT requirements demand the power-generation plant [3], [4] for the following conditions: 1) to remain connected to the grid, if line voltage is above the limit curve in Fig. 2 and 2) to help the power system to boost the voltage. To do so, a certain amount of reactive power has to be injected into the grid, as shown in Fig. 3. This amount of reactive power depends on the percentage of grid-voltage reduction during the dip and the system rated current. For dips with a voltage reduction larger than 50%, the full-rated current has to be delivered to the grid as reactive current, and no active power is injected into the grid.

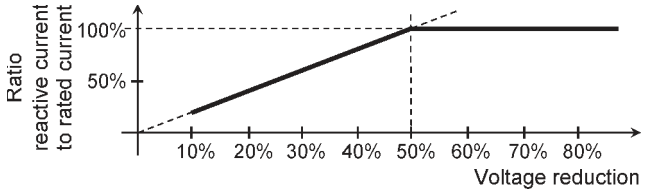


Fig. 3. Reactive current to be fed under a voltage dip.

Therefore, active and reactive power references have to be changed when a grid-voltage dip appears, accordingly with the requirement shown in Fig. 3. Grid-voltage-dip detection is needed in order to change the references. Two detections have to be performed concurrently: detection of negative-sequence voltages (asymmetrical dips) and detection of grid-voltage reduction (symmetrical dips).

## III. System Description and Equations

The system studied in this paper is shown in Fig. 4, where the NPC topology is connected to the grid through an inductor filter. A constant dc-link voltage is considered, in order to focus the analysis on the grid-side current-controller performance.

For the system shown in Fig. 1, in steady state, grid-side converter keeps constant the dc-link voltage with an appropriate controller (not considered in this paper, for simplicity) [16]–[18], [21], [22]. Under grid perturbation, the maximum active power that can be injected to the grid is reduced in proportion to the terminal-voltage reduction [21]. Moreover, this active power can be also limited by the LVRT requirements [3]–[5]. The power extracted from the generator can be reduced by means of the generator-side converter control as quickly as the grid-side converter, leading to speed increase in the generator due to the power mismatch between the mechanical input power and the electrical output power, even if pitch control is used to reduce the power extracted from the wind. This control can be used if the generator speed (and blades speed) is below the maximum admissible speed. If the generator-side converter control is not applied, an active power surplus is found in the dc-link, resulting in an unacceptable dc-link voltage increase [21]. To avoid this, back-to-back power converters are equipped with a dc-link-voltage limiter unit (dc-link brake chopper) [21]–[24], which can dissipate the active power surplus during the grid fault using braking resistors, and both converters can run relatively unaffected [21], [23].

In this scenario, by means of the generator-side control and/or the dc-link brake-chopper action, the dc-link voltage will be nearly constant and, subsequently, generator- and grid-side converters' control can be considered decoupled, as in steady state. Therefore, the assumption of constant dc-link done in this paper can be considered to be realistic and proper.

The state-space model in the positive and negative synchronous reference frames for the system shown in Fig. 4 is

$$\begin{aligned}\frac{d}{dt}i_{dp} &= \omega \cdot i_{qp} - \frac{R_L}{L}\cdot i_{dp} + \frac{1}{L}\cdot v_{VSIdp} - \frac{1}{L}\cdot v_{sdp}\\ \frac{d}{dt}i_{qp} &= -\omega \cdot i_{dp} - \frac{R_L}{L}\cdot i_{qp} + \frac{1}{L}\cdot v_{VSIqp} - \frac{1}{L}\cdot v_{sqp}\end{aligned} \quad (1)$$

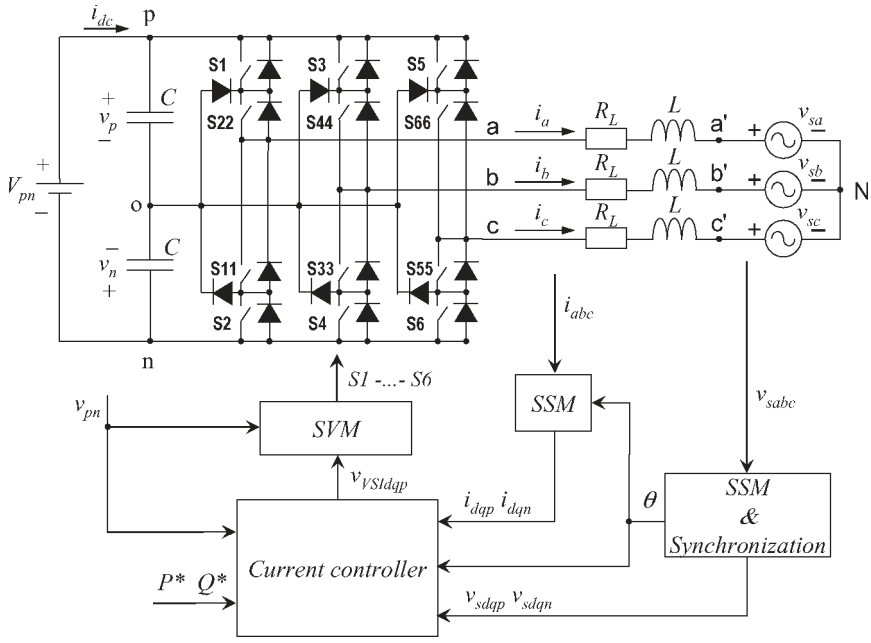


Fig. 4. System under study and control block diagram approach.

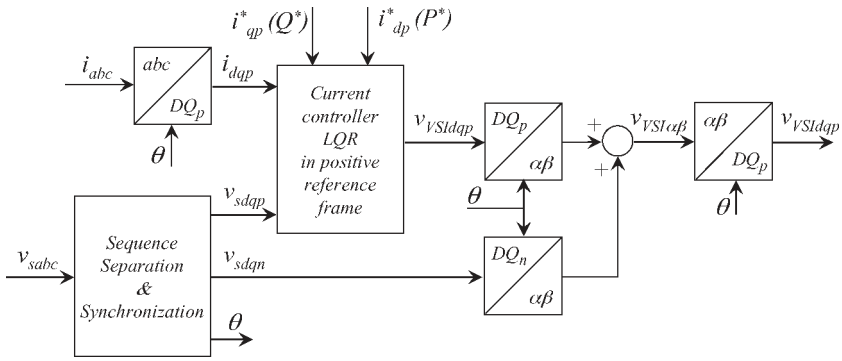


Fig. 5. Control block diagram for VCCF.

$$\frac{d}{dt}i_{dn} = -\omega \cdot i_{qn} - \frac{R_L}{L} \cdot i_{dn} + \frac{1}{L} \cdot v_{VSIdn} - \frac{1}{L} \cdot v_{sdn}$$
$$\frac{d}{dt}i_{qn} = \omega \cdot i_{dn} - \frac{R_L}{L} \cdot i_{qn} + \frac{1}{L} \cdot v_{VSIqn} - \frac{1}{L} \cdot v_{sqn} \quad (2)$$

where

| | |
|---|---|
| $i_{dp}, i_{qp}$ | positive-sequence $dq$ grid currents; |
| $i_{dn}, i_{qn}$ | negative-sequence $dq$ grid currents; |
| $v_{VSIdp}, v_{VSIqp}$ | positive-sequence $dq$ voltages generated at inverter terminals; |
| $v_{VSIdn}, v_{VSIqn}$ | negative-sequence $dq$ voltages generated at inverter terminals; |
| $v_{sdp}, v_{sqp}$ | positive-sequence $dq$ grid voltages; |
| $v_{sdn}, v_{sqn}$ | negative-sequence $dq$ grid voltages. |

The system (1) and (2) is linear and multivariable. Hence, the LQR [25] technique is well suited for the implementation of its control. The model is obtained using moving average operator for all variables over the switching period and $d$–$q$ transformation. Information about the dc-link neutral point is not included in the model because dc-link neutral-point voltage balance is achieved by means of the space-vector-modulation switching strategy [26].

A sequence-separation method (SSM) is needed to extract positive and negative sequences. Delayed-signal-cancellation (DSC) method is probably the best-suited SSM [13], [27] but produces an inaccurate sequence separation during $T/4$ ($T = 2\pi/\omega$ is the line period) after the beginning of any transient.

Grid-connected systems require the knowledge of the phase angle of the grid, for system-control purposes [28]. Phase-locked loop (PLL) working with an SSM guarantees angle precision when asymmetrical grid faults or unbalanced grid condition occur [29], [30]. For the implementation of the PLL, the most common approach is to align the "$d$"-axis of the synchronous reference frame with the positive-sequence vector of the grid voltage ($v_{sqp} = 0$).

## IV. Current Controllers Under Study

### A. Control Block Diagrams

Three current controllers are under study. The block scheme for the first controller is shown in Fig. 5, designated as vector

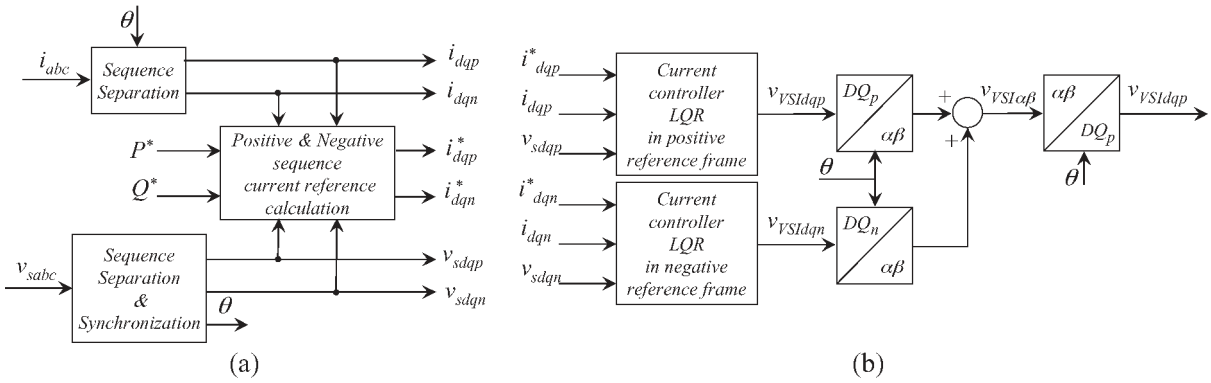


Fig. 6. Control block diagram for DVCC. (a) Stage 1. Sequence separation, synchronization, and current-reference calculation. (b) Stage 2. Current controllers in positive and negative reference frames.

current controller with feedforward of negative-sequence grid voltage (VCCF) in [13]. The current controller is implemented in the positive reference frame, while the negative-sequence grid voltage is fed-forward and added to the reference voltage given by the controller. Therefore, the voltage generated by the converter has exactly the same negative-sequence voltage as the grid voltage, and only positive-sequence currents (hence, balanced) flow to the grid through the filter. Current references can be easily calculated from active and reactive power references in the positive reference frame.

Both the second and third controllers are represented by the same control block diagram, shown in Fig. 6, and are defined as dual vector current controllers (DVCCs) [13]. This control approach has two stages. In the first stage [Fig. 6(a)], sequence separation, synchronization, and current-reference calculation are done. In the second stage [Fig. 6(b)], two current controllers are implemented in both the positive and negative reference frames. Different controller action can be achieved depending on the current-reference calculation [12], [14].

### *B. Two Different Current-Reference Calculations for DVCC*

Consider the apparent power at grid terminals calculated with positive- and negative-sequence components (3) expressed in matrix form (4). $P$ and $Q$ are the constant or average active and reactive power, respectively, while $P_{2c}$, $P_{2s}$, $Q_{2c}$, $Q_{2s}$ are the second-harmonic cosine and sine components of the active and reactive power, terms that appear when the three-phase system is not symmetrical and balanced [31]–[33].

The active power dissipated in the filter presents different terms: constant or average terms (5) or second-harmonic cosine (6) and sine (7) terms, given in [12] and [32].

Two different methods are found in [12] to calculate current references for DVCC, depending on how oscillating active powers are treated. The first method (DVCC1) calculates current references (8) by setting active and reactive power references $(P^*, Q^*)$ and by nullifying the oscillating active power delivered to the grid $(P^*_{2c} = P^*_{2s} = 0)$. In this case, the oscillating active power flows between the filter and the dc-link. In order to work with an invertible matrix ($4 \times 4$), oscillating reactive power $(Q_{2c}, Q_{2s})$ cannot be included in the current-reference calculation (8). Therefore, oscillating reactive power is not controlled and will flow through the system

$$\begin{aligned}\underline{S}_g &= (\underline{v}_{sdqp} \cdot e^{j\omega t} + \underline{v}_{sdqn} \cdot e^{-j\omega t}) \\ &\quad \cdot (\underline{i}_{sdqp} \cdot e^{j\omega t} + \underline{i}_{sdqn} \cdot e^{-j\omega t})^* \\ &= (P + P_{2c} \cdot \cos(2\omega t) + P_{2s} \cdot \sin(2\omega t)) \\ &\quad + j\,(Q + Q_{2c} \cdot \cos(2\omega t) + Q_{2s} \cdot \sin(2\omega t)) \end{aligned} \tag{3}$$

$$\begin{bmatrix} P \\ P_{2c} \\ P_{2s} \\ Q \\ Q_{2c} \\ Q_{2s} \end{bmatrix} = \begin{bmatrix} v_{sdp} & v_{sqp} & v_{sdn} & v_{sqn} \\ v_{sdn} & v_{sqn} & v_{sdp} & v_{sqp} \\ v_{sqn} & -v_{sdn} & -v_{sqp} & v_{sdp} \\ v_{sqp} & -v_{sdp} & v_{sqn} & -v_{sdn} \\ v_{sqn} & -v_{sdn} & v_{sqp} & -v_{sdp} \\ -v_{sdn} & -v_{sqn} & v_{sdp} & v_{sqp} \end{bmatrix} \cdot \begin{bmatrix} i_{dp} \\ i_{qp} \\ i_{dn} \\ i_{qn} \end{bmatrix} \tag{4}$$

$$\Delta P = R_L \cdot \left(i_{dp}^2 + i_{qp}^2 + i_{dn}^2 + i_{qn}^2\right) \tag{5}$$

$$\begin{aligned}\Delta P_{2c} &= 2R_L \cdot (i_{dp} \cdot i_{dn} + i_{qp} \cdot i_{qn}) \\ &\quad + 2\omega L \cdot (i_{dp} \cdot i_{qn} - i_{qp} \cdot i_{dn}) \end{aligned} \tag{6}$$

$$\begin{aligned}\Delta P_{2s} &= 2R_L \cdot (i_{dp} \cdot i_{dn} - i_{qp} \cdot i_{qn}) \\ &\quad + 2\omega L \cdot (-i_{dp} \cdot i_{qn} - i_{qp} \cdot i_{dn}) \end{aligned} \tag{7}$$

$$\begin{bmatrix} i^*_{dp} \\ i^*_{qp} \\ i^*_{dn} \\ i^*_{qn} \end{bmatrix} = \begin{bmatrix} v_{sdp} & v_{sqp} & v_{sdn} & v_{sqn} \\ v_{sdn} & v_{sqn} & v_{sdp} & v_{sqp} \\ v_{sqn} & -v_{sdn} & -v_{sqp} & v_{sdp} \\ v_{sqp} & -v_{sdp} & v_{sqn} & -v_{sdn} \end{bmatrix}^{-1} \cdot \begin{bmatrix} P^* \\ 0 \\ 0 \\ Q^* \end{bmatrix}. \tag{8}$$

The second method (DVCC2) calculates current references (9) by setting active and reactive power references $(P^*, Q^*)$ and by forcing the oscillating active power demanded by the filter to be delivered from the grid $(P^*_{2c} = -\Delta P_{2c}; P^*_{2s} = -\Delta P_{2s})$. Then, no oscillating active power flows between the dc-link and the filter

$$\begin{bmatrix} i^*_{dp} \\ i^*_{qp} \\ i^*_{dn} \\ i^*_{qn} \end{bmatrix} = \begin{bmatrix} v_{sdp} & v_{sqp} & v_{sdn} & v_{sqn} \\ v_{sdn} & v_{sqn} & v_{sdp} & v_{sqp} \\ v_{sqn} & -v_{sdn} & -v_{sqp} & v_{sdp} \\ v_{sqp} & -v_{sdp} & v_{sqn} & -v_{sdn} \end{bmatrix}^{-1} \cdot \begin{bmatrix} P^* \\ -\Delta P_{2c} \\ -\Delta P_{2s} \\ Q^* \end{bmatrix}. \tag{9}$$

### C. Current-Controller LQR Calculation

The positive-sequence grid currents $(i_{dp}, i_{qp})$ are controlled by the LQR regulator in VCCF controller, while two identical LQR regulators for the positive and negative reference frames are used to control positive $(i_{dp}, i_{qp})$- and negative $(i_{dn}, i_{qn})$-sequence grid currents, respectively, in the DVCC controller.

LQR is well suited for this application [19] because of the multivariable structure of the system (1) and (2). Using the state-space model of the system and a user-defined cost function, the LQR algorithm [26] returns a constant control matrix $[K]$ that minimizes the cost function by using the control law $[u] = -[K] \cdot [x]$ ($u$ are the control variables, and $x$ are the state variables).

The cost function $J$ is defined in (10). The integrals of the state variables $(I_{id}, I_{iq})$ have been included as new states in the state-space equation, in order to include integral action in the controller and cancel steady-state errors. The same cost function is used for the calculation of the positive-sequence control matrix $[K_p]$ and the negative-sequence control matrix $[K_n]$. This is the conventional approach.

The weights in the $[Q]$ and $[R]$ matrices in the cost function $J$ (10) are user-defined. An initial set of values is proposed. The controller calculation is performed by means of the MATLAB LQR built-in function. The system is simulated with the resulting control matrix or matrices, and the results are analyzed in light of the system-performance specifications. After an iterative process through simulations, a set of proper weights is found

$$\begin{aligned} J &= \begin{bmatrix} \hat{i}_d \\ \hat{i}_q \\ I\hat{i}_q \\ I\hat{i}_q \end{bmatrix}^{\mathrm{T}} \cdot [Q] \cdot \begin{bmatrix} \hat{i}_d \\ \hat{i}_q \\ I\hat{i}_q \\ I\hat{i}_q \end{bmatrix} + \begin{bmatrix} \widehat{v}_{VSId} \\ \widehat{v}_{VSIq} \end{bmatrix}^{\mathrm{T}} \cdot [R] \cdot \begin{bmatrix} \widehat{v}_{VSId} \\ \widehat{v}_{VSIq} \end{bmatrix} \\ &= \begin{bmatrix} \hat{i}_d \\ \hat{i}_q \\ I\hat{i}_q \\ I\hat{i}_q \end{bmatrix}^{\mathrm{T}} \cdot \begin{bmatrix} WP_d & 0 & 0 & 0 \\ 0 & WP_q & 0 & 0 \\ 0 & 0 & WI_d & 0 \\ 0 & 0 & 0 & WI_q \end{bmatrix} \cdot \begin{bmatrix} \hat{i}_d \\ \hat{i}_q \\ I\hat{i}_q \\ I\hat{i}_q \end{bmatrix} \\ &\quad + WR \cdot \begin{bmatrix} \widehat{v}_{VSId} \\ \widehat{v}_{VSIq} \end{bmatrix}^{\mathrm{T}} \cdot \begin{bmatrix} 1 & 0 \\ 0 & 1 \end{bmatrix} \cdot \begin{bmatrix} \widehat{v}_{VSId} \\ \widehat{v}_{VSIq} \end{bmatrix}. \end{aligned} \tag{10}$$

## V. Simulation and Experimental Validation

This section presents simulation and experimental results for the system shown in Fig. 4, using the specifications of a low-power laboratory system: $L = 10$ mH; $R_L = 0.5\ \Omega$; $C = 2200\ \mu$F; $V_{pn} = 100$ V; $V_{\mathrm{GRID}} = 37\ \mathrm{V_{RMS}}$; and $f = 50$ Hz.

The objectives of this section are as follows: 1) to evaluate the three current-controller strategies regarding to LVRT requirements and system performance; 2) to validate experimentally the proposed overall control-system approach; and 3) to validate the simulation environment developed to simulate the system shown in Fig. 4 and to calculate the LQR controller.

The control system has been implemented using a PC-embedded DSP (dSPACE 1104), with a sampling time $T_s = 200\ \mu$s. Hence, the switching frequency $(f_s)$ is set to 5 kHz. Discrete LQR controllers have been calculated for this sample frequency and specifications, using the procedure described in Section IV. The values for $[Q]$ and $[R]$ matrices shown in Table I have been used both for the simulations and for the experimental setup. The sample frequency has been also included within the simulations.

TABLE I
Weights in the LQR Cost Function for the Three Controllers With the Specifications of the Experimental Setup

| | $WP_d$ | $WP_q$ | $WI_d$ | $WI_q$ | $WR$ |
|---|---|---|---|---|---|
| **VCFF** | 1e3 | 1e3 | 1e5 | 1e5 | 1 |
| **DVCC1** | 1e3 | 1e3 | 1e2 | 1e2 | 1 |
| **DVCC2** | 1e2 | 1e2 | 1e3 | 1e3 | 1 |

The system with the three different controllers has been tested under a 70% grid-voltage-dip type B and a grid-voltage-dip type C with 50% voltage drop and 30° phase shift [7]. Simulations for the voltage-dip type B are shown in Fig. 7, whereas the corresponding experimental results are shown in Fig. 8. For the voltage-dip type C, simulations are shown in Fig. 9 and experimental results shown in Fig. 10. Both voltage dips have been generated with a duration of 60 ms. Grid voltages, grid currents, and instantaneous $(P(t), Q(t))$ and average $(P_{AV}, Q_{AV})$ active and reactive power delivered to the grid are depicted. Experimental results have been obtained from the DSP readings in all cases. In the simulations, the specifications are the same with the experimental system, and the dips have been generated at the same instant shown in the experimental results, in order to carry out a simple and direct comparison between simulations and experimental results. $P$ and $Q$ references are set to 50 W and 0 VAR in steady state. During the dip, the $P$ and $Q$ references are properly changed $(P^* = 0\ \mathrm{W}; Q^* = 70\ \mathrm{VAR})$ to meet the LVRT requirement [3], [4].

These references can be set to any value, with no restriction, in order to adapt them to the specific GCR of each country. Therefore, two transient effects take place concurrently: the voltage-dip transient and the reference change. The three controllers (VCCF, DVCC1, DVCC2) work under the same condition, to compare and to evaluate their performance.

The available grid voltages at the laboratory present significant harmonic distortion [Figs. 8(a), (d), and (g) and 10(a), (d), and (g)], leading to distorted grid currents [Figs. 8(b), (e), and (h) and 10(b), (e), and (h)]. However, the comparison with simulation results proves that the system performance is not substantially affected by this distortion. Controllers are robust enough to bear the distortion.

Dips have been generated in the laboratory by switching one grid phase from its rated voltage to a smaller voltage generated by a single-phase autotransformer, using two bidirectional electronic switches. Depending on the relative position between the mentioned system and the grid transformer, a dip type B or C is generated.

A first analysis of the results shows a slight slower transient operation for DVCC2 in comparison with VCCF and DVCC1. If weights in the LQR cost function are increased to achieve a faster DVCC2 control response, control variables will exceed switching-strategy limits, leading to the overmodulation region and system instability. A possible reason for this slow response

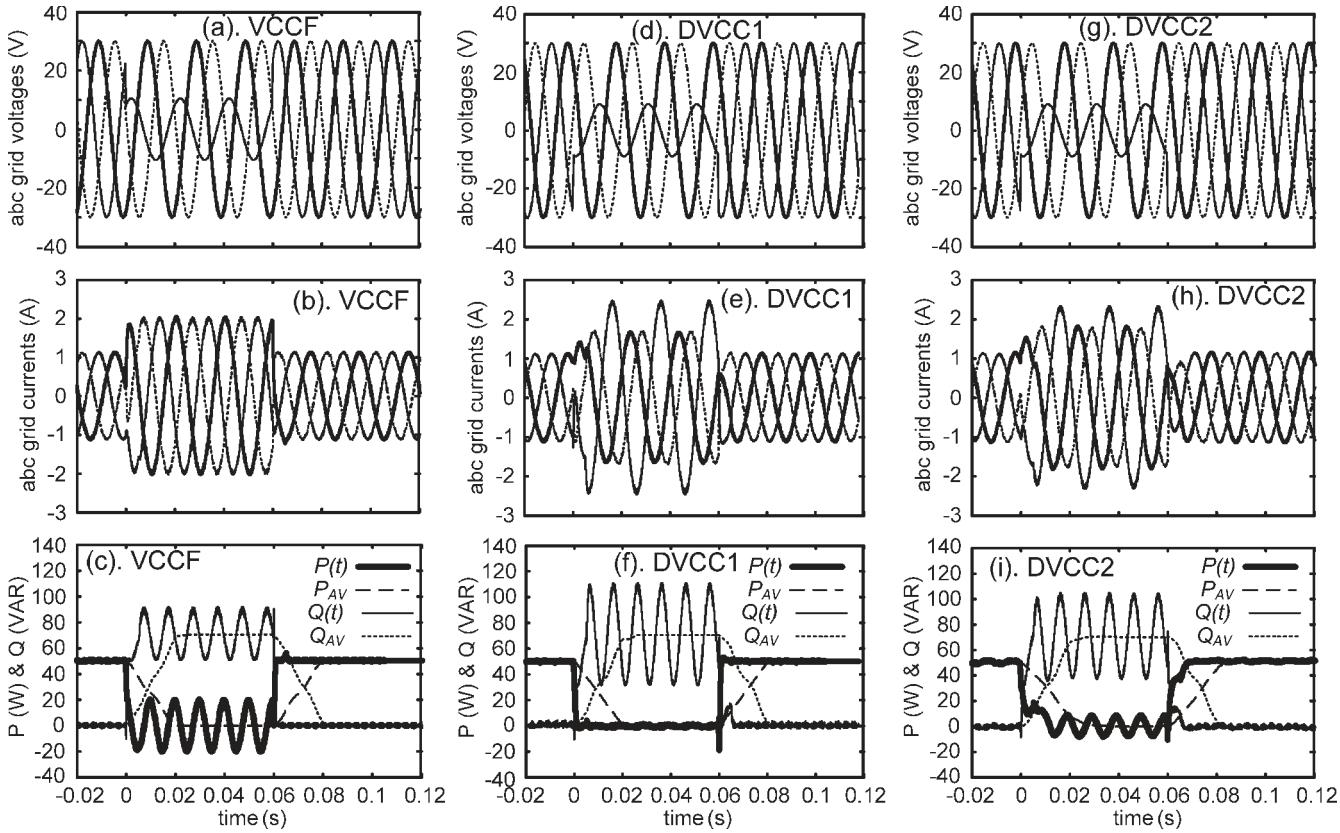


Fig. 7. Simulation results. Grid voltages, grid currents, and instantaneous and average active and reactive power for a 70% dip type B. (a)–(c) VCCF. (d)–(f) DVCC1. (g)–(i) DVCC2.

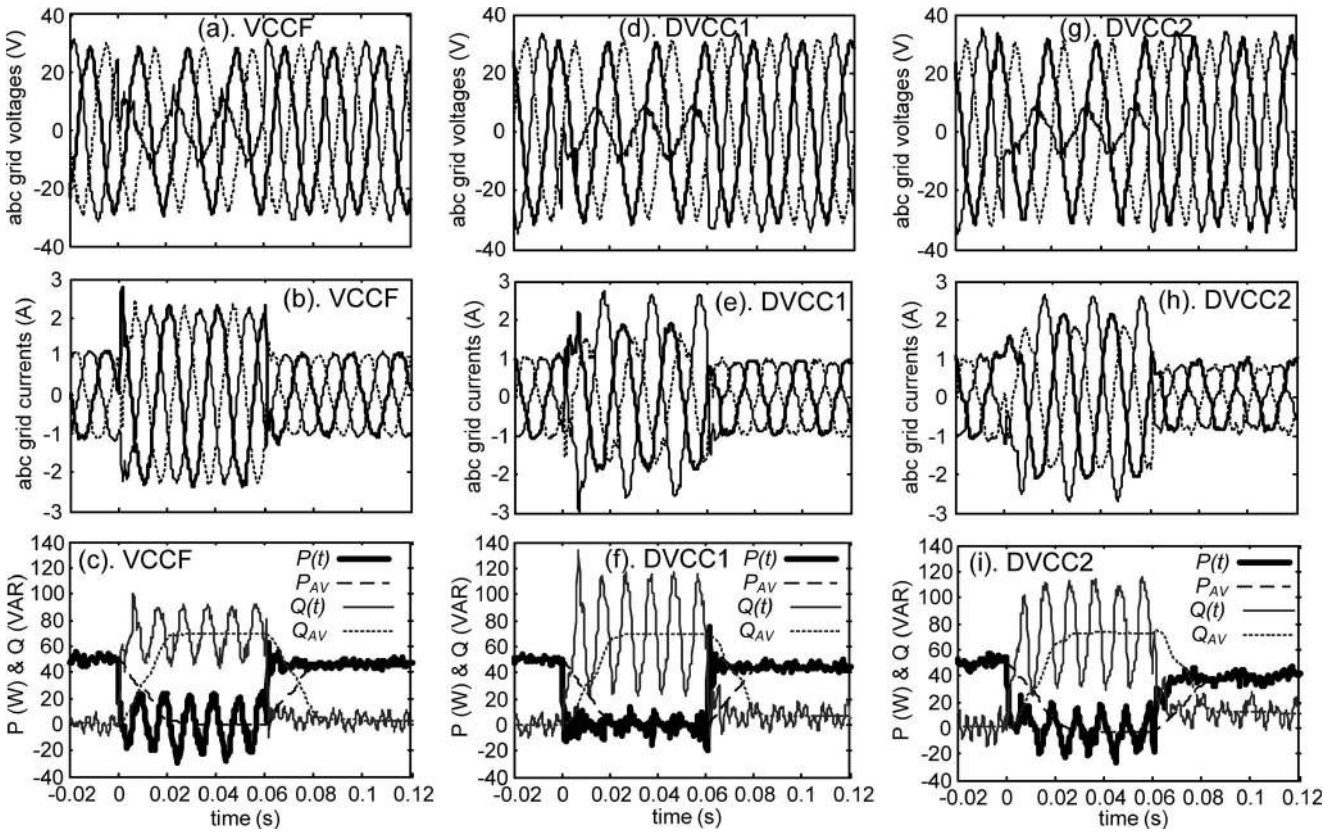


Fig. 8. Experimental results. Grid voltages, grid currents, and instantaneous and average active and reactive power for a 70% dip type B. (a)–(c) VCCF. (d)–(f) DVCC1. (g)–(i) DVCC2.

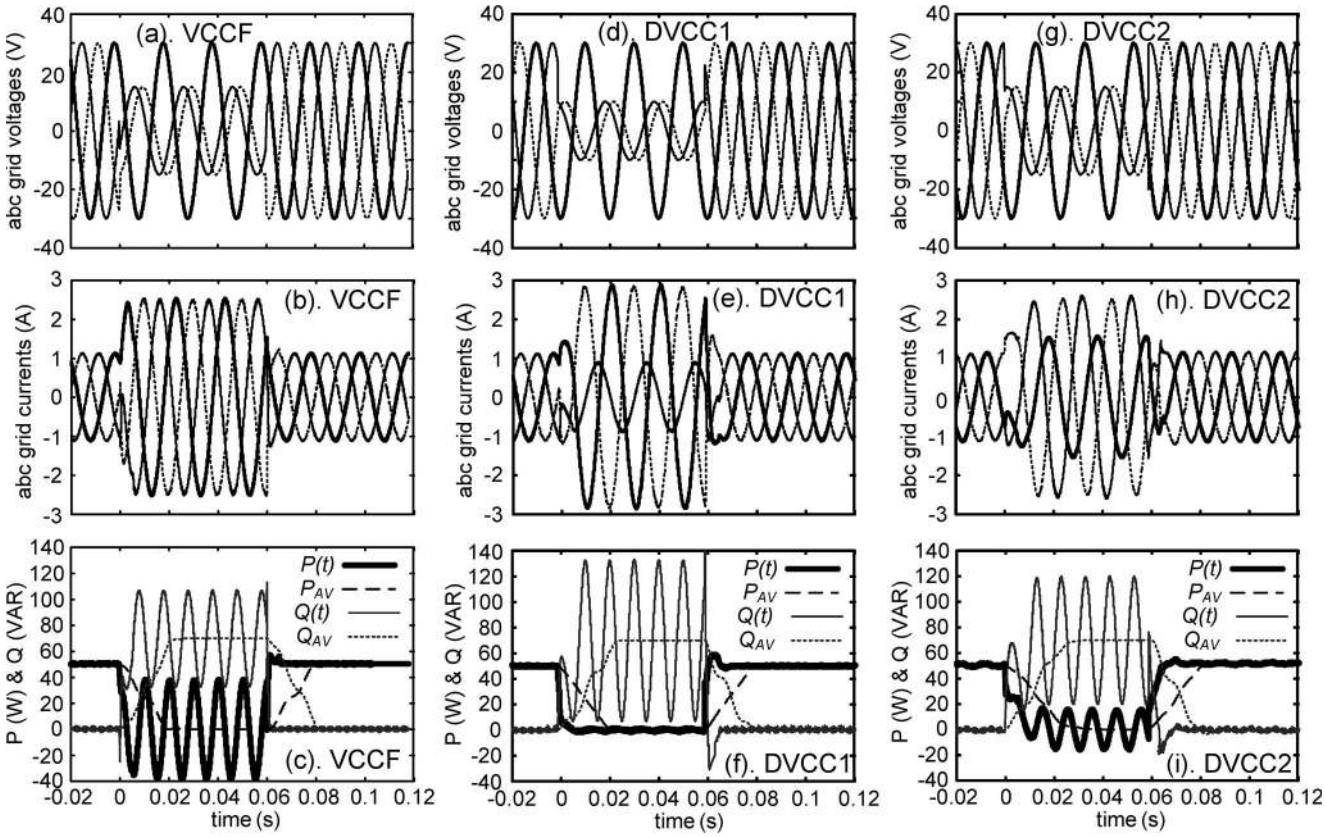


Fig. 9. Simulation results. Grid voltages, grid currents, and instantaneous and average active and reactive power for a 50% dip type C. (a)–(c) VCCF. (d)–(f) DVCC1. (g)–(i) DVCC2.

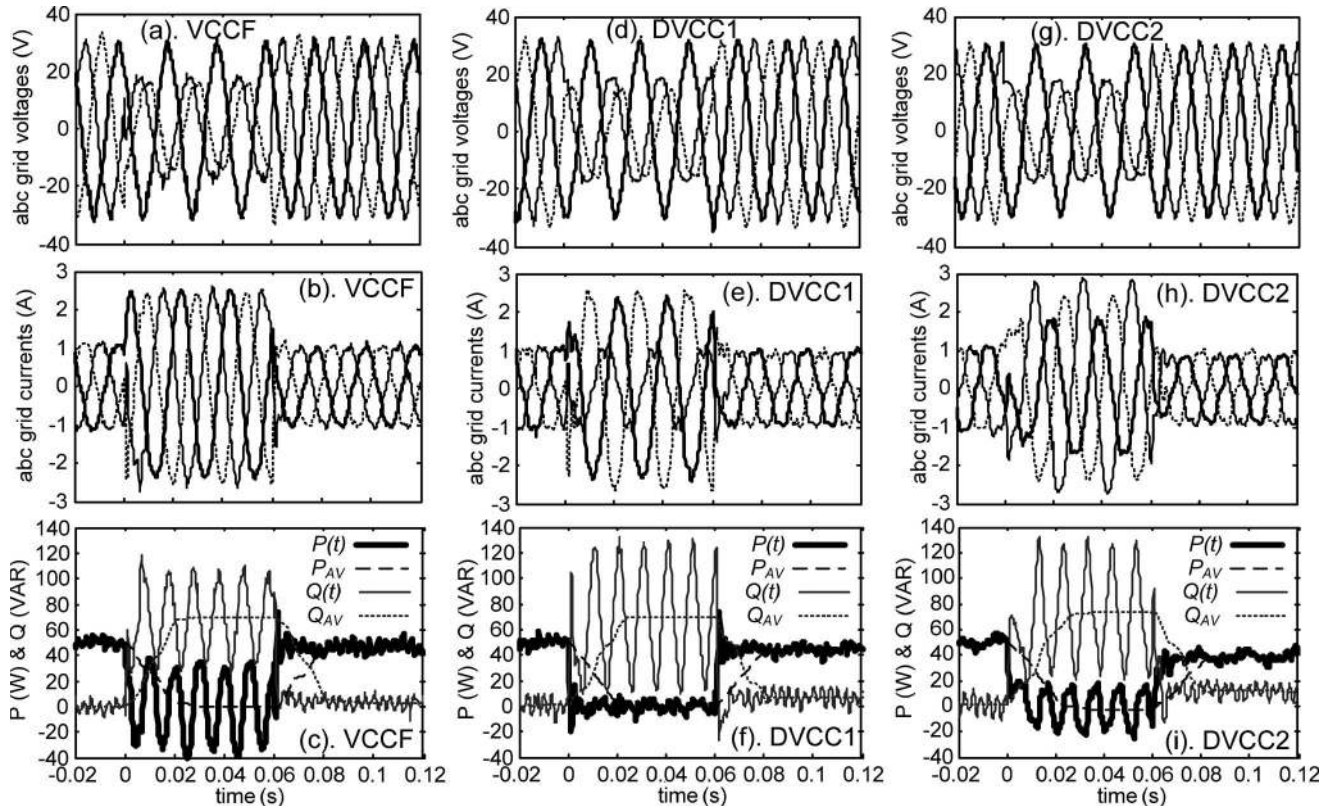


Fig. 10. Experimental results. Grid voltages, grid currents, and instantaneous and average active and reactive power for a 50% dip type C. (a)–(c) VCCF. (d)–(f) DVCC1. (g)–(i) DVCC2.

can be found in the oscillating power-reference calculation (6), (7), and (9), which depends on the actual current values.

VCCF gives symmetrical and balanced grid currents [Figs. 7–10(b)] and guarantees controlled current values for the three phases. Then, under any voltage dip, a balanced grid-current peak value can be set by the reference, avoiding filter saturation and line overcurrent. Unbalanced currents are found for DVCC1 and DVCC2 [Figs. 7–10(e) and (h)]. In addition, peak currents are larger than for VCCF, and the regulator does not directly control currents but power. This could lead to filter saturation or line overcurrent. Grid-current waveforms are slightly inaccurate for DVCC1 and DVCC2 only during the first 5 ms after dip occurrence and clearance because of the intrinsic DSC delay to separate symmetrical components. This delay is avoided when VCCF is used, because grid currents only present positive-sequence component. Hence, an SSM is not needed, and conventional $dq$ transformation is applied.

Average active and reactive power [Figs. 7–10(c), (f), and (i)] are regulated as LVRT requirement demands [3], [4] using any of the considered controller schemes. Only reactive power is delivered to the grid during the dip. From this point of view, no difference among controllers is found, apart from the slower response for DVCC2 aforementioned. Some steady-state error is found after the fault clearance for DVCC2 [Figs. 8(i) and 10(i)]. However, this error will not become a problem, because the active and reactive power recovery rates after fault clearance implemented in this paper exceeds by far that specified in the GCR [3], [4].

Oscillating active and reactive power are present for VCCF [Figs. 7–10(c)]. No oscillating active power is delivered to the grid for DVCC1, but larger oscillating reactive power is found [Figs. 7–10(f)]. The amplitude of these oscillations is given by the amount of negative-sequence grid voltages and currents, as shown in (3) and (4). In comparison with VCCF, DVCC2 [Figs. 7–10(i)] shows smaller oscillating active power but larger oscillating reactive power. Oscillating powers delivered to the grid can make more difficult the control of the network voltage and frequency under distorted condition. Nevertheless, all the three controllers meet the LVRT requirement. On the other hand, inaccuracies are present in the active and reactive power due to the DSC intrinsic delay, particularly for DVCC1 and DVCC2. For VCCF, DSC is only applied to grid voltages, reducing these deviations.

The time required by the DSC method to calculate the symmetrical components is very small, and it is included within the sampling time (200 $\mu$s) of the controller. Therefore, this calculation time does not affect the control dynamics. However, DSC presents an intrinsic delay of $T/4$, which does not affect under steady-state operation, but makes an inaccurate sequence separation during the first 5 ms (with $T = 20$ ms) after the appearance of any grid transient. During this interval of time, inaccurate values are fed back to the control system. The result of these inaccuracies can be observed in the currents and power performance, both in simulations and experimental results, during the 5 ms after the fault appearance and clearance. Despite of these inaccuracies due to DSC, the results obtained seem to be acceptable in all cases. The aforementioned delay in the DSC is also a common drawback in other SSMs [13], [27], [33].

TABLE II
SUMMARY OF CONTROL STRATEGIES PERFORMANCE

| | *VCCF* | *DVCC1* | *DVCC2* |
|---|---|---|---|
| **Grid currents balanced** | yes | no | no |
| **Grid currents peak controlled** | yes | no | no |
| **Grid currents SSM needed** | no | yes | yes |
| **Instant P ripple** | + | $\approx 0$ | – |
| **Instant Q ripple** | + | ++ | + |
| **Average P controlled** | yes | yes | yes |
| **Average Q controlled** | yes | yes | yes |
| **LVRT requirement verified** | yes | yes | yes |

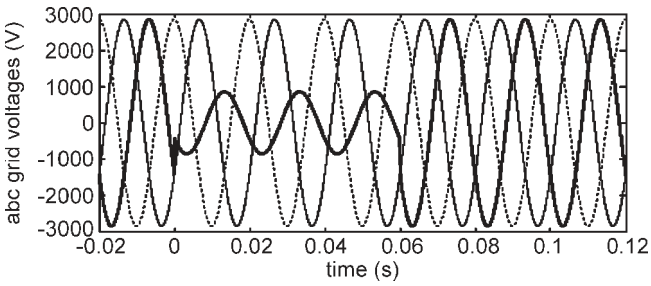


Fig. 11. Grid voltages. 70% dip type B.

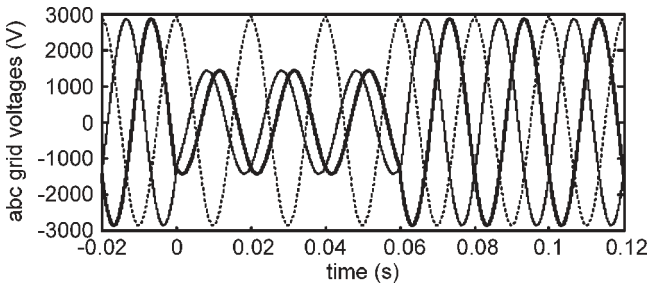


Fig. 12. Grid voltages. 50% dip type C with 30° phase shift.

Table II shows a summary of the performance for the three control strategies considered, deduced from both simulation and experimental results.

Because of the low-voltage level of the experimental prototype, it could be expected that the voltage drop of the power devices will influence the controller performance. However, this voltage drop can be an additional constant term added in each equation of the model (1) and (2). This term acts as a perturbation in the system, corrected by the integral action of the LQR controller. Results confirm this statement.

Finally, good agreement is found between simulations and experimental results. The main difference between simulations and experimental results is found on the grid-voltage harmonic content, which introduces ripple on $dq$ grid-voltage variables and some small inaccuracies in the control. Therefore, the simulation environment has been validated for controller calculation and system-performance simulation. Using this simulation environment, it is reasonable to consider that simulations with other specifications and/or under different condition will deliver accurate-enough system performance.

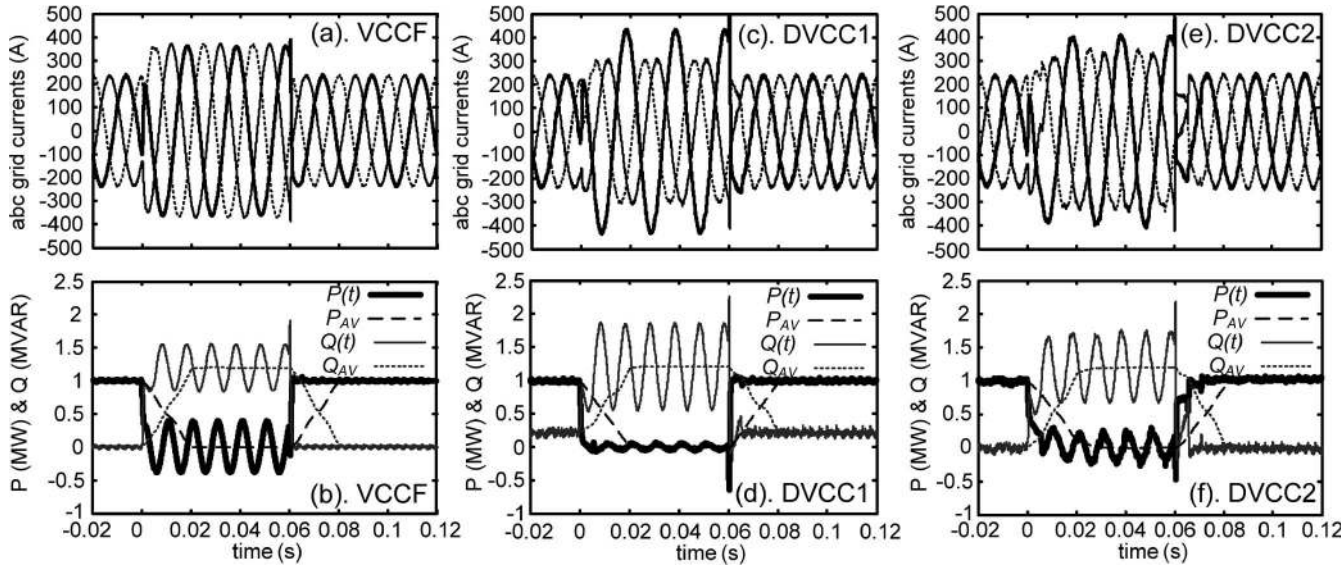


Fig. 13. Simulation results. Average grid currents and instantaneous and average active and reactive power for a 70% dip type B. (a), (b) VCCF. (c), (d) DVCC1. (e), (f) DVCC2.

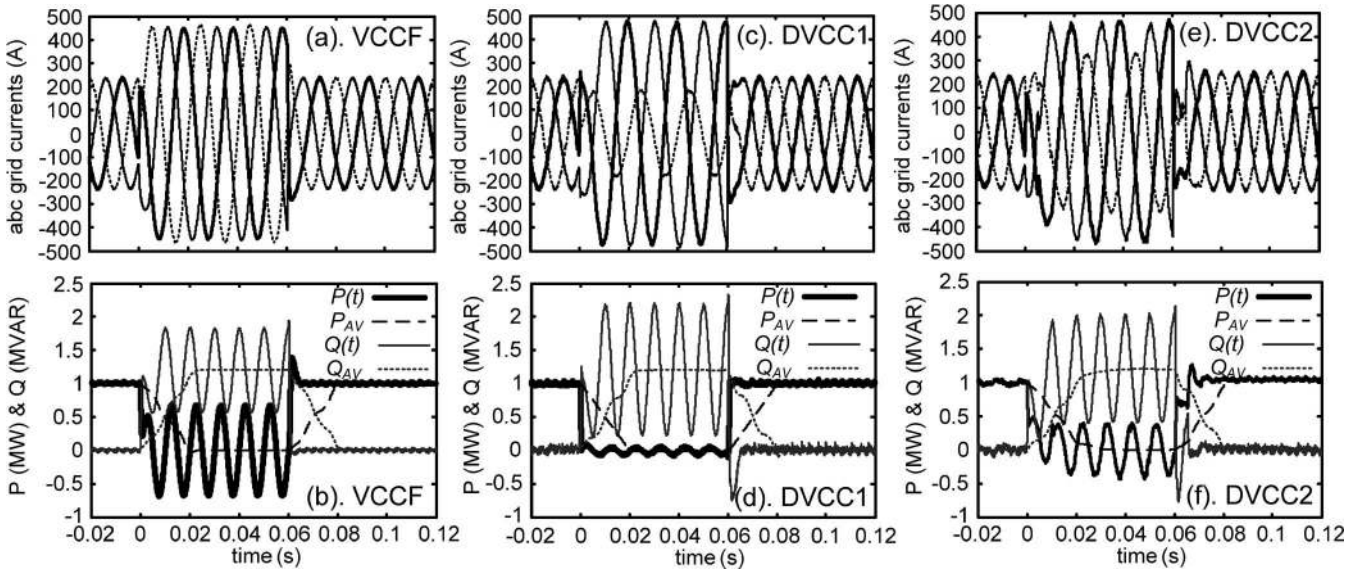


Fig. 14. Simulation results. Average grid currents and instantaneous and average active and reactive power for a 50% dip type C. (a), (b) VCCF. (c), (d) DVCC1. (e), (f) DVCC2.

## VI. Additional Simulation Results

In the previous section, the simulation environment has been validated by comparing simulations with experimental results using a low-power experimental setup. However, some results considering a high-power system are needed to give a more realistic view. For this reason, this section shows additional simulation results for the system in Fig. 4 with high voltage and power ratings.

The specifications for the simulated system in Fig. 4 in this section are as follows [18], [19]: $L = 0.5$ mH; $R_L = 0.1\ \Omega$; $C = 4700\ \mu$F; $V_{pn} = 6000$ V; $V_{\mathrm{GRID}} = 3500\ V_{\mathrm{RMS}}$; and $f = 50$ Hz.

The sampling time for the discrete LQR controllers is $T_s = 400\ \mu$s, and the switching frequency ($f_s$) is set to 2.5 kHz. For the sake of simplicity, the values for $[Q]$ and $[R]$ matrices in the previous section, shown in Table I, have been also used in this section, taking advantage of the LQR robustness [25]. However, in any case, it is suitable to calculate the LQR controllers considering the corresponding filter and sampling-time values, to obtain the most effective controller, and to avoid possible control system instabilities.

A 70% grid-voltage-dip type B (Fig. 11) and a 50% grid-voltage-dip type C (Fig. 12) have been simulated. $P$ and $Q$ references are set to 1 MW and 0 MVAR in steady state. During the dip, $P$ and $Q$ references are switched ($P^* = 0$ MW; $Q^* = 1.2$ MVAR) in order to deliver reactive current to the grid in accordance with the LVRT requirements.

Average grid currents are shown in Figs. 13(a), (c), and (e) and 14(a), (c), and (e). Due to the small filter value, the small switching frequency, and the large voltage values, actual grid

currents present significant ripple. The displayed grid currents are the actual grid currents averaged at the switching frequency ($f_s = 2.5$ kHz), in order to show clearer waveforms. No essential information is missed with this assumption.

Simulations presented in this section deliver similar results as in the preceding section, verifying the application of the considered controllers in high-power wind systems.

VCCF gives symmetrical and balanced grid currents [Figs. 13(a) and 14(a)], with a maximum value that can be precisely controlled by the regulator under any grid dip. Therefore, line overcurrent and/or filter saturation is avoided. Unbalanced grid currents are found for DVCC1 and DVCC2 [Figs. 13(b) and (c) and 14(b) and (c)], with an uncontrolled grid-current peak value higher than for VCCF. Currents must be kept under the maximum admissible value of the semiconductors at any time. This can lead to a power-reference reduction. For DVCC1 and DVCC2, grid-current waveforms are inaccurate the first 5 ms after dip occurrence and clearance, due to the DSC delay.

All three controllers regulate average active and reactive power [Figs. 13(b), (d), and (f) and 14(b), (d), and (f)] as the LVRT requirement demands, and only average reactive power is delivered to the grid during the dip. In comparison with VCCF and DVCC1, DVCC2 presents a slower response, agreeing with the results in the preceding section.

Figs. 13(b) and 14(b) show oscillating active and reactive power for VCCF. For DVCC1 [Figs. 13(d) and 14(d)], no oscillating active power is delivered to the grid but presents the largest oscillating reactive power. In comparison with VCCF, DVCC2 [Figs. 13(f) and 14(f)] shows smaller oscillating active power but larger oscillating reactive power.

## VII. Conclusion

Three controls dealing with symmetrical components have been evaluated in terms of meeting the LVRT requirement and other system-performance features (instant active and reactive power ripple, balanced grid currents, maximum grid-current control).

Current controllers have been implemented using the LQR control technique, in order to take advantage of the multivariable nature of the system.

Results show that all three controllers fulfill LVRT requirements, but all the control objectives cannot be achieved concurrently. Each control scheme (VCCF or DVCC) gives different comparative advantages in terms of system performance. VCCF control scheme prioritizes to deliver balanced grid currents, whereas DVCC control scheme prioritizes to nullify oscillating active power flow. Therefore, controller selection depends on the system constraints and the performance features to be prioritized.

Good agreement is found between simulations and experimental results. Hence, controllers can be calculated through simulation, and accurate system performance can be predicted. The main difference between simulations and experimental results is found on the grid-voltage harmonic content, which introduces ripple on $dq$ grid-voltage variables and some small inaccuracies in the control.

## References


[1] Wind Energy Barometer European Commission 2008 (EurObserv'ER), *Systèmes Solaires*, no. 183, pp. 75–99, Feb. 2008.

[2] *Resolution on the Commission communication: Energy for the future: renewable sources of energy—WhitePaper for a Community Strategy and Action Plan*. COM(97)0599 C4-0047/98. European Commission Official Journal, C 210, pp. 0215, Jul. 6, 1998.

[3] Red Eléctrica, *Procedimiento de operación 12.3: Requisitos de respuesta frente a huecos de tensión de las instalaciones de producción en régimen especial*, Oct. 2006, Spain. [Online]. Available: www.ree.es

[4] "High and extra high voltage," *E.ON Netz*, Aug. 2003, Germany. [Online]. Available: www.eon-netz.com

[5] I. Erlich and U. Bachmann, "Grid code requirements concerning connection and operation of wind turbines in Germany," in *Proc. IEEE Power Eng. Soc. Gen. Meet.*, Jun. 12–16, 2005, vol. 2, pp. 1253–1257.

[6] I. Erlich, W. Winter, and A. Dittrich, "Advanced grid requirements for the integration of wind turbines into the German transmission system," in *Proc. IEEE Power Eng. Soc. Gen. Meet.*, Jun. 2006, vol. 1, pp. 18–22.

[7] M. Bollen, *Understanding Power Quality Problems: Voltage Sags and Interruptions*. New York: IEEE Press, 1999.

[8] J. Rodríguez, J. Dixon, J. Espinoza, J. Pontt, and P. Lezana, "PWM regenerative rectifiers: State of the art," *IEEE Trans. Ind. Electron.*, vol. 52, no. 1, pp. 5–22, Feb. 2005.

[9] J. Rodríguez, J. Pontt, G. Alzamora, N. Becker, R. Huerta, S. Kouro, P. Cortés, and P. Lezana, "Resonances in a high power active front end rectifier system," *IEEE Trans. Ind. Electron.*, vol. 52, no. 1, pp. 482–488, Feb. 2005.

[10] F. Blaabjerg, R. Teodorescu, M. Liserre, and A. Timbus, "Overview of control and grid synchronization for distributed power generation systems," *IEEE Trans. Ind. Electron.*, vol. 53, no. 5, pp. 1398–1409, Oct. 2006.

[11] F. Magueed and J. Svensson, "Control of VSC connected to the grid through LCL-filter to achieve balanced currents," in *Conf. Rec. IEEE IAS Annu. Meeting*, Oct. 2–6, 2005, vol. 1, pp. 572–578.

[12] F. Magueed, A. Sannino, and J. Svensson, "Transient performance of voltage source converter under unbalanced voltage dips," in *Proc. IEEE PESC*, Jun. 20–25, 2004, vol. 2, pp. 1163–1168.

[13] G. Saccomando and J. Svensson, "Transient operation of grid-connected voltage source converter under unbalanced conditions," in *Conf. Rec. IEEE IAS Annu. Meeting*, Sep. 30–Oct. 4, 2001, vol. 4, pp. 2419–2424.

[14] E. Bueno, "Optimización del Comportamiento de un Convertidor de Tres Niveles NPC Conectado a la Red Eléctrica," Ph.D. dissertation, Universidad de Alcalá, Alcalá de Henares, Spain, Feb. 2005.

[15] J. Carrasco, L. Garcia-Franquelo, J. T. Bialasiewicz, E. Galván, R. C. Portillo-Guisado, M. A. Martín Prats, J. I. León, and N. Moreno-Alfonso, "Power-electronic systems for the grid integration of renewable energy sources: A survey," *IEEE Trans. Ind. Electron.*, vol. 53, no. 4, pp. 1002–1016, Aug. 2006.

[16] R. Portillo, M. M. Prats, J. I. Leon, J. A. Sanchez, J. M. Carrasco, E. Galvan, and L. G. Franquelo, "Modeling strategy for back-to-back three-level converters applied to high-power wind turbines," *IEEE Trans. Ind. Electron.*, vol. 53, no. 5, pp. 1483–1491, Oct. 2006.

[17] M. Chinchilla, S. Arnaltes, and J. C. Burgos, "Control of permanent-magnet generators applied to variable-speed wind-energy systems connected to the grid," *IEEE Trans. Energy Convers.*, vol. 21, no. 1, pp. 130–135, Mar. 2006.

[18] A. Faulstich, J. K. Steinke, and F. Wittwer, "Medium voltage converter for permanent magnet wind power generators up to 5 MW," in *Proc. 11th Eur. Conf. Power Electron. Appl. EPE*, Dresden, Germany, Sep. 11–14, 2005, vol. 1, pp. 1–10.

[19] P. Maibach, A. Faulstich, M. Eichler, and S. Dewar, *Full-Scale Medium-Voltage Converters for Wind Power Generators up to 7 MW*. Turgi, Switzerland: ABB, Feb. 2007. [Online]. Available: www.abb.com

[20] S. Alepuz, S. Busquets-Monge, J. Bordonau, J. Gago, D. Gonzalez, and J. Balcells, "Interfacing renewable energy sources to the utility grid using a three-level inverter," *IEEE Trans. Ind. Electron.*, vol. 53, no. 5, pp. 1504–1511, Oct. 2006.

[21] J. F. Conroy and R. Watson, "Low-voltage ride-through of a full converter wind turbine with permanent magnet generator," *IET Renew. Power Gener.*, vol. 1, no. 3, pp. 182–189, Sep. 2007.

[22] M. Fatu, C. Lascu, G. D. Andreescu, R. Teodorescu, F. Blaabjerg, and I. Boldea, "Voltage sags ride-through of motion sensorless controlled PMSG for wind turbines," in *Conf. Rec. IEEE IAS Annu. Meeting*, Sep. 23–27, 2007, vol. 1, pp. 171–178.

[23] M. Eichler, P. Maibach, and A. Faulstich, "Full size voltage converters for 5 MW offshore wind power generators," in *Proc. EWEC*, Mar. 31–Apr. 3, 2008, vol. 1, pp. 1–10. Poster 161.
[24] "PCS 6000 Wind datasheet," *Medium Voltage Full Power Frequency Converter for Wind Turbines*, ABB, Turgi, Switzerland. [Online]. Available: www.abb.com
[25] P. Dorato, C. Abdallah, and V. Cerone, *Linear-Quadratic Control: An Introduction*. Englewood Cliffs, NJ: Prentice-Hall, 1995.
[26] S. Busquets, "A novel pulsewidth modulation for the comprehensive neutral-point voltage control in the three-level three-phase neutral-point-clamped dc–ac converter," Ph.D. dissertation, Tech. Univ. Catalunya, Barcelona, Spain, Feb. 2006.
[27] S. Alepuz, S. Busquets, J. Bordonau, J. Pontt, C. Silva, and J. Rodríguez, "Fast on-line symmetrical components separation method for synchronization and control purposes in three phase distributed power generation systems," in *Proc. 12th Eur. Conf. Power Electron. Appl. EPE*, Aalborg, Denmark, Sep. 2–5, 2007, pp. 1–10.
[28] A. Timbus, M. Liserre, R. Teodorescu, and F. Blaabjerg, "Synchronization methods for three phase distributed power generation systems. An overview and evaluation," in *Proc. IEEE PESC*, Jun. 11–16, 2005, pp. 2474–2481.
[29] V. Kaura and V. Blasko, "Operation of a phase locked loop system under distorted utility conditions," *IEEE Trans. Ind. Appl.*, vol. 33, no. 1, pp. 58–63, Jan./Feb. 1997.
[30] L. Barbosa, D. Rodrigues da Costa, and M. Aredes, "Analysis and software implementation of a robust synchronizing PLL circuit based on the PQ theory," *IEEE Trans. Ind. Electron.*, vol. 53, no. 6, pp. 1919–1926, Dec. 2006.
[31] Y. Suh, V. Tijeras, and T. Lipo, "A control method in dq synchronous frame for PWM boost rectifier under generalized unbalanced operating conditions," in *Proc. IEEE PESC*, Jun. 2002, vol. 3, pp. 1425–1430.
[32] J. K. Kang and S. K. Sul, "Control of unbalanced voltage PWM converter using instantaneous ripple power feedback," *IEEE Trans. Ind. Electron.*, vol. 46, no. 5, pp. 953–959, Oct. 1999.
[33] P. Rodriguez, A. Timbus, R. Teodorescu, M. Liserre, and F. Blaabjerg, "Flexible active power control of distributed power generation systems during grid faults," *IEEE Trans. Ind. Electron.*, vol. 54, no. 5, pp. 2583–2592, Oct. 2007.

**Salvador Alepuz** (S'98–M'03) was born in Barcelona, Spain. He received the M.Sc. and Ph.D. degrees in electrical and electronic engineering from the Technical University of Catalonia (UPC), Barcelona, Spain, in 1993 and 2004, respectively.

Since 1994, he has been an Associate Professor with the Mataró School of Engineering, UPC. From 2006 to 2007, he was with the Departamento de Electrónica, Universidad Técnica Federico Santa María, Valparaíso, Chile, where he was involved in postdoctoral research. He is currently developing his research with the Department of Electronic Engineering, Technical University of Catalonia. His fields of interest are in multilevel conversion and ac power conversion applied to renewable energy systems.

**Sergio Busquets-Monge** (S'99–M'06) was born in Barcelona, Spain. He received the B.Sc. degree in electrical engineering from the Technical University of Catalonia, Barcelona, in 1999, the M.S. degree in electrical engineering from Virginia Polytechnic Institute and State University, Blacksburg, in 2001, and the Ph.D. degree in electrical engineering from the Technical University of Catalonia, in 2006.

From 2001 to 2002, he was with Crown Audio, Inc. He is currently an Associate Professor with the Department of Electronic Engineering, Technical University of Catalonia. His research interests include multilevel conversion and converter integration.

**Josep Bordonau** (S'87–M'89) received the M.Sc. and Ph.D. degrees (with honors) in electrical engineering from the Technical University of Catalonia, Barcelona, Spain, in 1984 and 1990, respectively.

He was a Lecturer and an Assistant Professor with the Department of Electronic Engineering, Technical University of Catalonia, where he has been an Associate Professor since 1991. He has been active in more than 25 research projects with international companies and institutions. He has authored more than 70 journal and conference papers. His fields of interest are in multilevel conversion and ac power conversion applied to renewable energy systems and energy management systems.

Dr. Bordonau is a member of the IEEE Technical Committee on Distributed Generation.

**Juan A. Martínez-Velasco** (M'83) was born in Barcelona, Spain. He received the M.Sc. degree in 1975 and the Ph.D. degree in 1982, both from the Technical University of Catalonia (UPC), Barcelona, Spain.

He is currently a Professor with the Department of Electrical Engineering, Technical University of Catalonia. His teaching and research interests include transmission and distribution, power system analysis, and ElectroMagnetic Transients Program (EMTP) applications.

**César A. Silva** (S'01–M'02) was born in Temuco, Chile, in 1972. He received the M.Sc. degree in civil electronic engineering from the Universidad Técnica Federico Santa María (UTFSM), Valparaiso, Chile, in 1998, and the Ph.D. degree from the University of Nottingham, Nottingham, U.K., in 2003. His Ph.D. thesis was entitled "Sensorless vector control of surface mounted permanent magnet machines without restriction of zero frequency."

In 1999, he was granted the Overseas Research Students Awards Scheme to join as a postgraduate research student the Power Electronics Machines and Control Group, University of Nottingham. Since 2003, he has been a Lecturer with the Departamento de Electrónica, UTFSM, where he teaches electric machines theory, power electronics, and ac machine drives. His main research interests include sensorless vector control of ac machines and control of static converters.

**Jorge Pontt** (M'00–SM'04) received the Engineer and M.S. degrees in electrical engineering from the Universidad Técnica Federico Santa María (UTFSM), Valparaíso, Chile, in 1977.

Since 1977, he has been a Professor with the Department of Electrical Engineering and the Departamento de Electrónica, UTFSM, within the R&D and graduate programs in power electronics. He leads the Laboratory for Reliability and Power Quality, UTFSM, and is currently the Director of Millennium Nucleus on Industrial Electronics and Mechatronics, UTFSM. He has had scientific stays at the Technische Hochschule Darmstadt, Darmstadt, Germany, from 1979 to 1980; the University of Wuppertal, Wuppertal, Germany, in 1990; and the University of Karlsruhe, Karlsruhe, Germany, from 2000 to 2001. He is a Cofounder of ETT Ltd., Chile, which is a spin-off company related to instrumentation for large grinding mills. He is the coauthor of the software Harmonix, which is used in harmonic studies in electrical systems. He is also a Consultant in the mining industry and energy processing, particularly in the design and application of high-power applications, power electronics, drives, instrumentation systems, power quality, and electromagnetic-compatibility issues, with management of more than 80 consulting and R&D projects. He has published more than 100 refereed journal and conference proceedings papers. He is the coauthor of nine patent applications (four conceded).

Prof. Pontt was appointed by the IEEE as an Eminent Engineer in the year 2008 in Region 9 (Latin America).

**José Rodríguez** (M'81–SM'94) received the Engineer degree in electrical engineering from the Universidad Técnica Federico Santa Maria (UTFSM), Valparaíso, Chile, in 1977, and the Dr.-Ing. degree in electrical engineering from the University of Erlangen, Erlangen, Germany, in 1985.

Since 1977, he has been with the Departamento de Electrónica, UTFSM, where from 2001 to 2004, he was the Director of the Department of Electronic Engineering, from 2004 to 2005, was Vice Rector of Academic Affairs, since 2005, has been the Rector, and currently, is a Professor. During his sabbatical leave in 1996, he was with the Mining Division, Siemens Corporation, Santiago, Chile. He has extensive consulting experience in the mining industry, particularly in the application of large drives such as cycloconverter-fed synchronous motors for SAG mills, high-power conveyors, and controlled ac drives for shovels and power-quality issues. He has directed more than 40 R&D projects in the field of industrial electronics. He has coauthored more than 250 journal and conference papers and contributed one book chapter. His research group has been recognized as one of the two centers of excellence in engineering in Chile from 2005 to 2008. His main research interests include multilevel inverters, new converter topologies, and adjustable-speed drives.

Dr. Rodríguez has been an active Associate Editor for the IEEE Power Electronics and IEEE Industrial Electronics Societies since 2002. He was the recipient of the Best Paper Award from the IEEE TRANSACTIONS ON INDUSTRIAL ELECTRONICS in 2007.